

# Spin relaxation in graphite due to spin-orbital-phonon interaction from first-principles density-matrix approach

Junqing Xu<sup>1,\*</sup>

<sup>1</sup>*Department of Physics, Hefei University of Technology, Hefei, Anhui, China*

(Dated: August 23, 2024)

We predict “intrinsic” spin relaxation times ( $T_1$ ) of graphite due to spin-orbit-phonon interaction, i.e., the combination of spin-orbit coupling and electron-phonon interaction, using our developed first-principles density-matrix approach. We obtain ultralong  $T_1$ , e.g.,  $\sim 600$  ns at 300 K, which leads to ultralong in-plane spin diffusion length  $\sim 110$   $\mu\text{m}$  within the drift-diffusion model. Our prediction sets the upper bound of  $T_1$  of graphite at each given temperature and Fermi level. The anisotropy ratios of  $T_1$  or values of  $T_{1z}/T_{1x}$  are found small and around 0.6. We examine the applicability of the well-known Elliot-Yafet (EY) relation, which declares that spin relaxation rate  $T_{1\alpha}^{-1}$  ( $\alpha = x, y, z$ ) is proportional to the product of the ensemble average of spin mixing parameter  $\langle b_\alpha^2 \rangle$  and carrier relaxation rate  $\tau_p^{-1}$ . Our numerical tests suggest that the EY relation works qualitatively if the degeneracy threshold  $t^{\text{deg}}$  for evaluating  $b_\alpha^2$  is relatively large (not much smaller than or comparable to  $k_B T$ ), e.g.,  $10^{-3}$  eV or larger, but fails if  $t^{\text{deg}}$  is too tiny (much smaller than  $k_B T$ ), e.g.,  $10^{-6}$  eV or smaller.

## I. INTRODUCTION

Spin lifetime  $\tau_s$ , including spin relaxation time  $T_1$  and (ensemble) spin dephasing time ( $T_2^*$ )  $T_2$ , and spin diffusion length  $l_s$  are key parameters for spintronic device applications, which aim to achieve the next generation of low-power electronics by making use of the spin degree of freedom.[1, 2] In spintronic devices,  $\tau_s$  and  $l_s$  of materials in spin transport channels are typically required long enough for stable detection and manipulation of spin. Due to the weak spin-orbit coupling (SOC) and negligible hyperfine interaction, carbon materials and nanomaterials such as graphene[3], carbon nanotubes[4] and graphite nanostructures[5], are expected to have long  $\tau_s$  and  $l_s$  and have been considered as promising candidates of spintronic materials. Up to  $\sim 10$   $\mu\text{s}$   $\tau_s$ , corresponding to hundreds of  $\mu\text{m}$   $l_s$ , was predicted for perfect suspended graphene.[6, 7] However, much shorter experimental values of  $\tau_s$ , 100 ps to 12 ns at room temperature, were reported, due to extrinsic origins such as impurities, substrates, etc.[3, 6]

Recently, ultralong 100 ns  $T_1$  of graphite at room temperature was obtained in ESR measurements by Markus et al. in Ref. 8. Since  $2T_1$  sets up the upper bound of  $\tau_s$  and  $l_s$  is known proportional to  $\tau_s$ , [1, 2] the knowledge of  $T_1$  is critical to spintronic applications. Remarkably, they also found highly anisotropic  $T_1$  with  $T_{1z}/T_{1x}$  up to 10, which is advantageous to efficient control of spin transport. However, due to the existence of various non-magnetic and magnetic impurities in realistic samples and possible Larmor precession induced by the orbital Zeeman effect in ESR measurements, the experimental data of  $T_1$  may be considerably lower than the ideal or intrinsic values due to spin-orbit-phonon interaction, i.e., the combination of spin-orbital coupling and

electron-phonon (e-ph) interaction. Therefore, theoretical predictions of intrinsic  $T_1$  are urgently needed to guide the future improvements of  $T_1$ .

Moreover, in the work of Markus et al., the simple Elliot-Yafet (EY) relation[1, 9] was employed to analyze the anisotropy of  $T_1$ . The EY relation declares that  $T_{1\alpha}^{-1}$  ( $\alpha = x, y, z$ ) is proportional to the product of the ensemble average of spin mixing parameter  $\langle b_\alpha^2 \rangle$  and carrier relaxation rate  $\tau_p^{-1}$ , and typically  $T_{1\alpha}^{-1} \sim 4 \langle b_\alpha^2 \rangle \tau_p^{-1}$ . Hereinafter, we name such quantitative estimate of  $T_1$  as  $T_{1\alpha}^{\text{EY}}$ . Based on the EY relation, the authors concluded that the high anisotropy of  $T_1$  is possibly attributed to the high anisotropy of spin-mixing parameter  $b^2$ . However, they only evaluated  $b_{kn}^2$  (state-resolved  $b^2$ ) at some k-points along the  $M$ - $K$ - $\Gamma$  path, where the anisotropy of  $b_{kn}^2$  varies from 0.5 to  $\sim 3 \times 10^6$ , but had not obtained the Fermi-surface averaged values  $\langle b^2 \rangle$ . More crucially, the applicability of the EY relation to graphite is problematic due to the following issue: The band structure of graphite contains multiple band-crossing points and four-fold degenerate regions near Fermi surface. Since  $b_{kn}^2$  is evaluated within the degenerate subspace, the value of  $b_{kn}^2$  is sensitive to the choice of the degeneracy threshold  $t^{\text{deg}}$ , if the state ( $k, n$ ) is close to the band-crossing point or in a near-degeneracy region. Therefore,  $\langle b_\alpha^2 \rangle$  and accordingly  $T_{1\alpha}^{\text{EY}}$  becomes strongly  $t^{\text{deg}}$  dependent, which is unphysical. Additionally, the EY relation is derived based on the assumptions of small  $b^2$  and slow variation of  $b_{kn}^2$  over wavevector, which are however not satisfied in their work. Therefore, it is urgent to simulate  $T_1$  directly via advanced *ab initio* methods and examine the applicability of the EY relation.

In this work, we apply our developed first-principles density-matrix dynamics (FPDM) approach[10–12] with self-consistent SOC and quantum description of the electron-phonon scattering, to simulate intrinsic  $T_1$  of graphite due to spin-orbit-phonon interaction at various temperatures and Fermi levels ( $E_F$ ). FPDM approach

\* jqxu@hfut.edu.cn

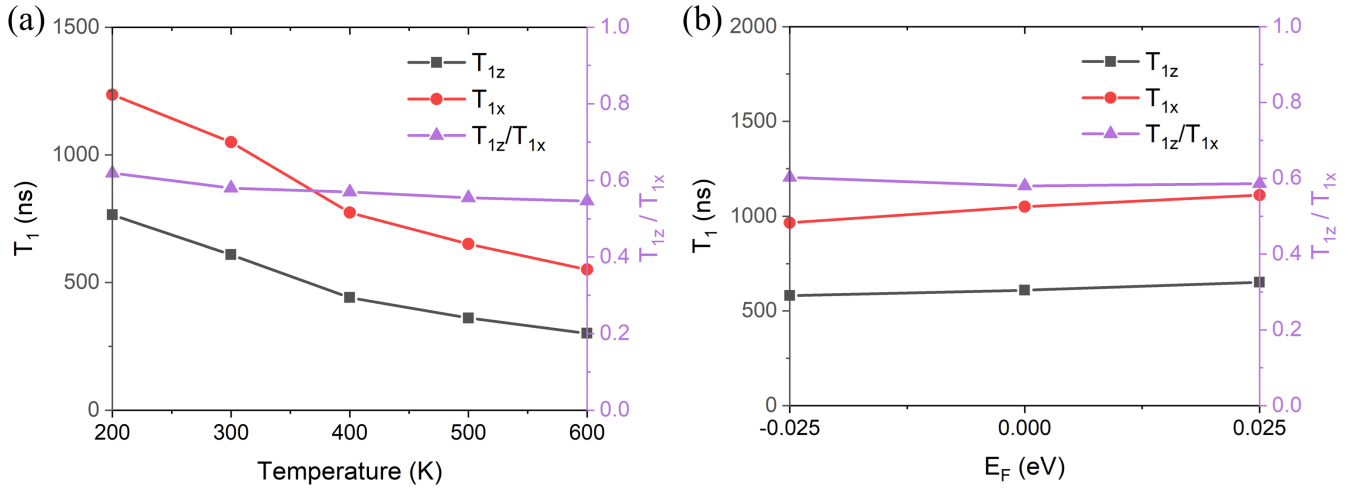


FIG. 1. Theoretical results of  $T_1$  and its anisotropy of graphite calculated by FPDM approach (a) at different temperatures with Fermi level  $E_F=0$  and (b) with different  $E_F$  at 300 K.

was applied to disparate materials including silicon, (bcc) iron, transition metal dichalcogenides (TMDs), graphene-hBN, GaAs and CsPbBr<sub>3</sub>, in good agreement with experiments.[10, 13] We then compare our FPDM results of  $T_1$  with results from the EY relation -  $T_1^{\text{EY}}$ , to gain mechanistic insights of spin relaxation in graphite.

## II. METHODS

### A. The density matrix master equation and spin lifetime

We solve the quantum master equation of density matrix  $\rho(t)$  as the following:[11, 14]

$$\frac{d\rho_{12}(t)}{dt} = -\frac{i}{\hbar} [H_e, \rho(t)]_{12} + \left( \frac{1}{2} \sum_{345} \left\{ \begin{array}{l} [I - \rho(t)]_{13} P_{32,45} \rho_{45}(t) \\ - [I - \rho(t)]_{45} P_{45,13}^* \rho_{32}(t) \end{array} \right\} + H.C. \right), \quad (1)$$

Eq. 1 is expressed in the Schrödinger picture, where the first and second terms on the right side of the equation relate to the coherent dynamics and the scattering processes within Born-Markov approximation respectively.  $H_e$  is the electronic Hamiltonian.  $[H, \rho] = H\rho - \rho H$ . H.C. is Hermitian conjugate. The subindex, e.g., “1” is the combined index of k-point and band. The weights of k-points must be considered when doing sum over k-points.  $P$  is the generalized scattering-rate matrix for the e-ph scattering, computed from the e-ph matrix elements and energies of electrons and phonons. Details of  $P$  are given in Appendix A.

Starting from an initial density matrix  $\rho(0)$  prepared with a net spin, we evolve  $\rho(t)$  through Eq. 1 for a long

enough time. We then obtain the excess spin observable  $S^{\text{ex}}(t)$  from  $\rho(t)$  and extract  $T_1$  from  $S^{\text{ex}}(t)$ . See details in Appendix B.

### B. Spin-mixing parameter $b^2$ and the EY relation

Due to time-reversal and spatial inversion symmetries of graphite (and each layer of it), every two bands of graphite form a Kramers degenerate pair,[1] so that spin-up/down is well defined along an arbitrary axis  $\hat{\mathbf{r}}$  by diagonalizing the corresponding spin matrix  $s_{\mathbf{r}} = \mathbf{s} \cdot \hat{\mathbf{r}}$  in degenerate subspaces. Therefore, spin relaxation in graphite is dominated by EY mechanism, i.e., caused by spin-flip transitions. For EY spin relaxation,  $T_1^{-1}$  is often well described by Fermi’s-golden-rule-like (FGR-like) formulas (Eqs. 22 and 23 in Appendix C.2) and qualitatively satisfies the EY relation described below.

#### 1. Spin-mixing parameter $b^2$

Suppose the spin of a state “1” is highly polarized along  $i$  direction. Then in general, the wavefunction of state “1” can be written as  $\Psi_1(\mathbf{r}) = a_{\alpha,1}(\mathbf{r})\alpha + b_{\alpha,1}(\mathbf{r})\beta$ , where  $a$  and  $b$  are the coefficients of the large and small components of the wavefunction, and  $\alpha$  and  $\beta$  are spinors (one up and one down for direction  $i$ ). Define  $a_{\alpha,1}^2 = \int |a_{\alpha,1}(\mathbf{r})|^2 d\mathbf{r}$  and  $b_{\alpha,1}^2 = \int |b_{\alpha,1}(\mathbf{r})|^2 d\mathbf{r}$ , then  $a_{\alpha,1}^2 > b_{\alpha,1}^2$  and  $b_{\alpha,1}^2$  is just spin-mixing parameter of state “1” along direction  $\alpha$ . [15, 16]

$$a_{\alpha,1}^2 + b_{\alpha,1}^2 = 1, \quad (2)$$

$$0.5(a_{\alpha,1}^2 - b_{\alpha,1}^2) = |S_{\alpha,1}^{\text{exp}}|, \quad (3)$$

where  $S_{\alpha,1}^{\text{exp}}$  is the spin expectation value of state “1” along the direction  $\alpha$ , and is an eigenvalue of the degeneracy projection of  $s_{\alpha}$  within the degenerate subspace

containing state “1”. From the above equations,

$$b_{\alpha,1}^2 = 0.5 - |S_{\alpha,1}^{\text{exp}}|. \quad (4)$$

Since  $S^{\text{exp}}$  depends on the degeneracy threshold  $t^{\text{deg}}$ ,  $b^2$  is also  $t^{\text{deg}}$  dependent. According to our discussions in Appendix C.3, a too small  $t^{\text{deg}}$  (such as  $10^{-6}$  eV or smaller) may be problematic in certain cases, while a larger  $t^{\text{deg}}$  (such as  $10^{-3}$  eV or larger) leads to reasonable results.

## 2. The EY relation

For EY spin relaxation,  $T_1^{-1}$  may be well described by FGR with spin-flip transitions. Thus,  $T_1^{-1}$  is qualitatively proportional to  $|g^{\uparrow\downarrow}|^2$  with  $g^{\uparrow\downarrow}$  the spin-flip scattering matrix element. Similarly,  $\tau_p^{-1} \propto |g^{\uparrow\uparrow}|^2$  with  $g^{\uparrow\uparrow}$  the spin-conserving scattering matrix element. Therefore, we have

$$T_1^{-1}/\tau_p^{-1} \propto |g^{\uparrow\downarrow}|^2 / |g^{\uparrow\uparrow}|^2. \quad (5)$$

According to Refs. 9, 17, 18,  $|g^{\uparrow\downarrow}|^2 / |g^{\uparrow\uparrow}|^2 \sim b^2$ , so that

$$T_1^{-1}/\tau_p^{-1} \sim \langle b^2 \rangle. \quad (6)$$

Practically, we use the following approximate relation[9]

$$T_1^{-1}/\tau_p^{-1} = 4 \langle b^2 \rangle. \quad (7)$$

This is called the EY relation in this work. Note that the EY relation is a rough relation and may lead to huge errors for some materials.[13, 16]

## III. RESULTS AND DISCUSSIONS

### A. $T_1$ from FPDM approach

We first show  $T_1$  results calculated by FPDM approach at different temperatures and  $E_F$  in Fig. 1. We obtain ultralong  $T_1$  in a wide range of temperatures and  $E_F$ . At 300 K and  $E_F=0$ ,  $T_{1z}$  and  $T_{1x}$  can reach 609 and 1050 ns respectively, if we only consider spin relaxation due to spin-orbit-phonon interaction. The magnitude of  $T_1$  is found decreasing with temperature and increasing slightly with  $E_F$ . On the other hand, the anisotropy ratio of  $T_1 - T_{1z}/T_{1x}$  is found around 0.55-0.6 and insensitive to temperature and  $E_F$ . More analysis of theoretical results of  $T_1$  are given below in the next subsection.

In recent ESR experiments[8],  $T_{1z} \sim 100$  ns and  $T_{1x} \sim 10$  ns at room temperature were reported. Thus, our FPDM approach predicts much longer  $T_1$  but much smaller anisotropy ratio ( $T_{1z}/T_{1x}$ ). The differences may be attributed to the following reasons: (i) There exist non-magnetic and magnetic impurities in experimental

samples. The existence of the impurities will reduce the magnitude of  $T_1$  and possibly change the anisotropy of  $T_1$ . (ii) Finite magnetic fields are applied in ESR measurements. Due to the orbital Zeeman effect, corresponding to the Hamiltonian  $H_k^{Z,\text{orb}} = \mu_B \mathbf{B} \cdot \mathbf{L}_k$  with  $\mathbf{L}_k$  the orbital angular momentum operator matrix, k-dependent Larmor precession processes may be induced by external magnetic field.[13] These processes possibly cause an additional spin relaxation channel. The effects of impurities and  $H_k^{Z,\text{orb}}$  on spin lifetimes are however hard to simulate and beyond the scope of this work.

Within the drift-diffusion model, spin-diffusion length of  $s_\alpha$  along the direction  $\beta$  of a non-magnetic metal can be estimated as  $l_{s_\alpha\beta} = \sqrt{\tau_p v_{F\beta}^2 T_{1\alpha}}$ , [8] where  $v_{F\beta}$  is the Fermi velocity along the direction  $\beta$ . Thus, with *ab initio* results of  $\tau_p$  (196 fs) and  $v_{F\beta}$  ( $v_{Fx} \approx 3.4 \times 10^5$  m/s), we obtain ultralong in-plane spin diffusion lengths  $l_{s_{zx}} \sim 117$   $\mu\text{m}$  and  $l_{s_{xx}} \sim 154$   $\mu\text{m}$  at 300 K. These values are several times longer than the reported experimental  $l_s$  of graphite up to  $\sim 30$   $\mu\text{m}$  at room temperature[3, 19] and make graphite a promising candidate of spintronic materials. The out-of-plane spin diffusion lengths are shorter and our estimates are  $l_{s_{zz}} \sim 12$   $\mu\text{m}$  and  $l_{s_{xz}} \sim 16$   $\mu\text{m}$  at 300 K with theoretical  $v_{Fz} \approx 3.5 \times 10^4$  m/s.

### B. Results related to the EY relation

As discussed in Sec. II B, spin relaxation in graphite at zero magnetic field should be caused by EY mechanism and can be qualitatively described by the EY relation (Eq. 7). Therefore, to improve the understandings of FPDM results of  $T_1$  (Fig. 1 and the above subsection), we next study the spin mixing parameter  $b^2$  and  $T_1$  results estimated by the EY relation.

In Fig. 2, we show band structure and the calculated k-resolved spin mixing parameter  $b_{\alpha,k}^2$  ( $\alpha = x, z$ ) of graphite.  $b_{\alpha,k}^2$  is the band average of  $b_{\alpha,kn}^2$  at a k-point (See the caption of Fig. 2). Due to time-reversal and spatial inversion symmetries, every two bands of graphite form a Kramers degenerate pair.[1] The band structure of graphite is found rather complicated: There are 8 bands near  $E_F$ . Moreover, there exist multiple band-crossing points, which are four-fold degenerate, near the  $K$ - $H$  line. For example, along the  $M$ - $K$ - $\Gamma$  line, there are two band-crossing points - one very close to  $K$  and another at  $K_2$  a little away from  $K$ .

According to the discussions in Sec. II B,  $b_{\alpha,kn}^2$  is computed from  $s_\alpha^{\text{deg}}$  - the degeneracy projection of the spin operator matrix  $s_\alpha$  within the degenerate subspace containing the state  $(k, n)$ . Therefore,  $b_{\alpha,k}^2$  can be  $t^{\text{deg}}$  dependent. Indeed, from Fig. 2(c)-(e), we find that  $b_{x,k}^2$  are very sensitive to  $t^{\text{deg}}$  near  $K$  and  $K_2$  (band-crossing points shown in Fig. 2(b)), although  $b_{z,k}^2$  at all k-points and  $b_{x,k}^2$  at other k-points (away from  $K$  and  $K_2$ ) are stable against  $t^{\text{deg}}$  and close to  $8.8 \times 10^{-8}$  and  $1.75 \times 10^{-7}$

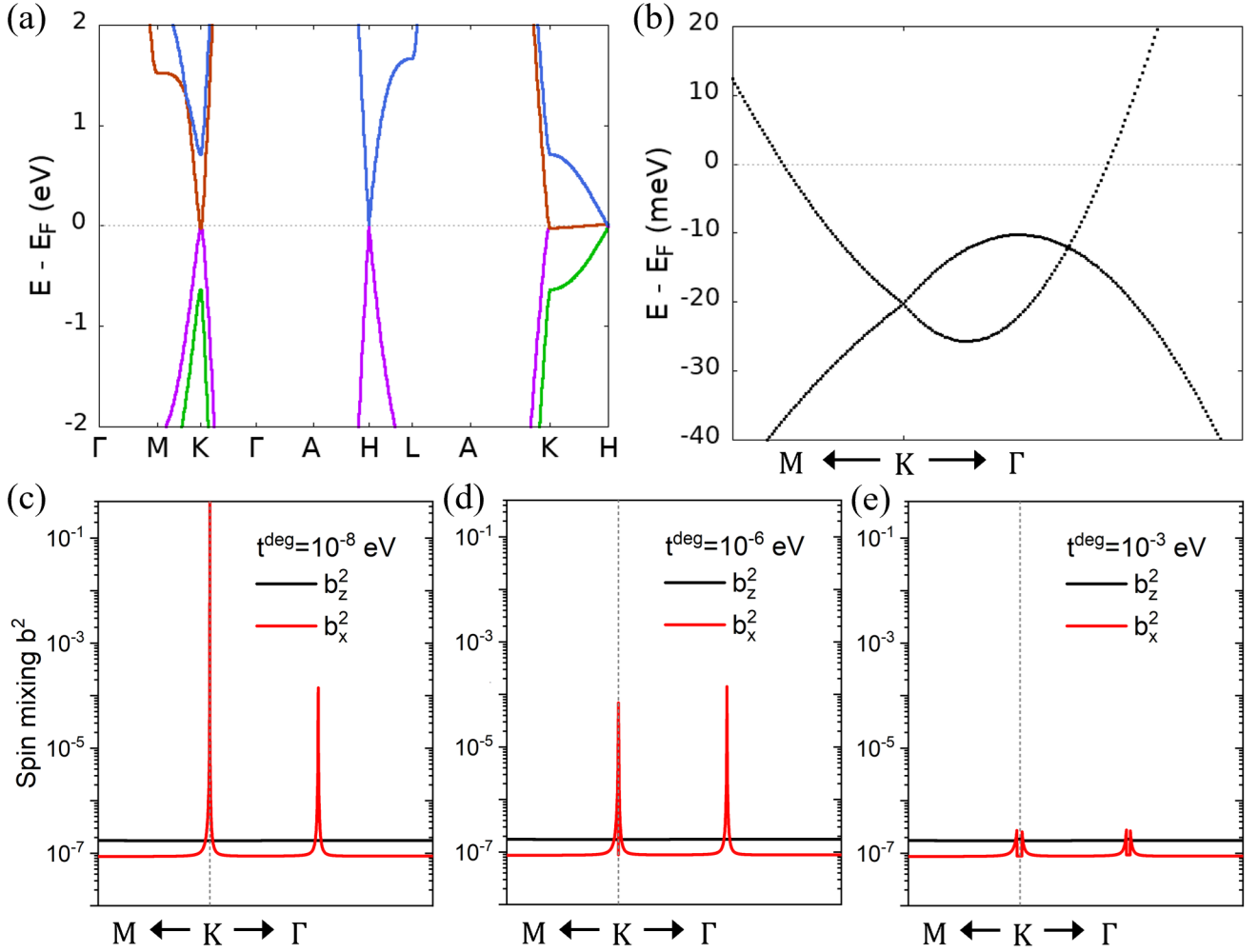


FIG. 2. (a) Band structure of graphite. (b) Band structure around  $K$  along  $M$ - $K$ - $\Gamma$ . (c) The  $k$ -resolved spin mixing parameter  $b_{\alpha,k}^2$  calculated with the degeneracy threshold  $t^{\text{deg}}=10^{-8}$  eV of  $k$ -points around  $K$  along  $M$ - $K$ - $\Gamma$ .  $b_k^2$  is defined as  $b_{\alpha,k}^2 = \frac{\sum_n f'_{kn} b_{\alpha,kn}^2}{\sum_n f'_{kn}}$ , where  $f'_{kn}$  is the derivative of the Fermi-Dirac distribution function of state  $(k, n)$  and  $b_{\alpha,kn}^2$  is the state-resolved spin-mixing parameter. (d) and (e) are  $b_{\alpha,k}^2$  calculated with  $t^{\text{deg}}$  of  $10^{-6}$  and  $10^{-3}$  eV respectively.

respectively. With  $t^{\text{deg}} \leq 10^{-6}$  eV, the curve of  $b_{x,k}^2$  has two sharp peaks at  $K$  and near  $K_2$  with the peak amplitudes  $\geq 10^{-4}$ . With  $t^{\text{deg}} = 10^{-8}$  eV, the maximum value of  $b_{x,k}^2$  is quite large and only slightly small than 0.5 (at  $K$ ). Our results of  $b_{\alpha,k}^2$  with  $t^{\text{deg}} = 10^{-8}$  eV are almost the same as Ref. 8. The large magnitudes of  $b_{x,k}^2$  indicate that  $s_{x,k}$  cannot be safely replaced by  $s_{x,k}^{\text{deg}}$  with  $t^{\text{deg}} \leq 10^{-6}$  eV, since the off-diagonal element of  $s_{x,k}$  is large between two states with a finite but tiny energy difference ( $\leq 10^{-6}$  eV). On the other hand, with relatively large  $t^{\text{deg}}$  of  $10^{-3}$  eV,  $b_{z,k}^2$  and  $b_{x,k}^2$  at all  $k$ -points are tiny ( $< 3 \times 10^{-7}$ ), indicating that  $s_{x,k} \approx s_{x,k}^{\text{deg}}$  if  $t^{\text{deg}} \geq 10^{-3}$  eV.

In Fig. 3(a), we show Fermi-surface averaged values  $\langle b_{\alpha}^2 \rangle$  with different  $t^{\text{deg}}$ . It can be seen that with relative large  $t^{\text{deg}}$  of  $10^{-3}$  eV,  $\langle b_z^2 \rangle$  and  $\langle b_x^2 \rangle$  are of order  $10^{-7}$  and not very sensitive to temperature (and also  $E_F$  as checked). However, with  $t^{\text{deg}} = 10^{-6}$  eV,  $\langle b_x^2 \rangle$  become

much larger and of order  $10^{-3}$ , while  $\langle b_z^2 \rangle$  are still small. See the additional details concerning the  $k$ -point convergence of  $\langle b_{\alpha}^2 \rangle$  simulations in Appendix D and Fig. 4.

With  $\langle b_{\alpha}^2 \rangle$  and *ab initio*  $\tau_p$  shown in Fig. 3(b) due to the e-ph scattering, we estimate spin relaxation times using the EY relation, called  $T_1^{\text{EY}}$  (Fig. 3(c)). With large  $t^{\text{deg}}$  of  $10^{-3}$  eV, we find that the EY relation qualitatively captures the magnitude and temperature dependence of  $T_1$ , i.e.,  $T_1^{\text{EY}}$  and  $T_1$  from FPDM approach have the same order of magnitude at different temperatures and their temperature dependences are quite similar. Since  $\langle b_{\alpha}^2 \rangle$  is weakly temperature dependent, the temperature dependences of  $T_1$  and  $\tau_p$  can be attributed to the same reason: With increasing temperature, the phonon occupations are increased, so that both the spin-flip and spin-conserving e-ph scattering strengths are enhanced, which correspond to larger  $T_1^{-1}$  and  $\tau_p^{-1}$ . On the other, with tiny  $t^{\text{deg}}$  of  $10^{-6}$  eV,  $T_{1x}^{\text{EY}}$  values are found faster

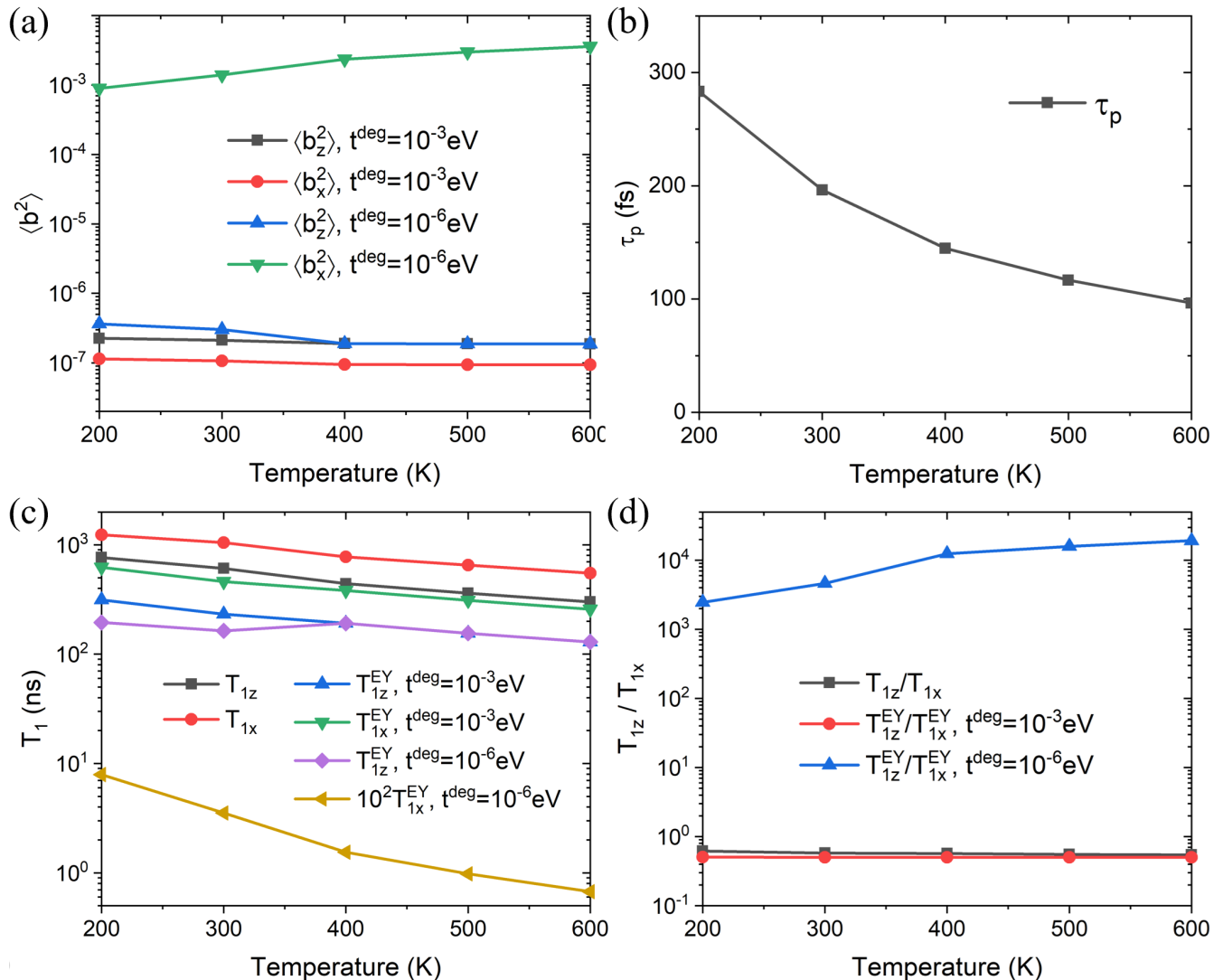


FIG. 3. Theoretical analysis related to the EY relation. (a) The Fermi-surface averaged spin mixing parameter along the directions  $z$  and  $x$  -  $\langle b_z^2 \rangle$  and  $\langle b_x^2 \rangle$  as a function of temperature with different  $t^{\text{deg}}$ . (b) Carrier lifetime  $\tau_p$ . (c) Spin relaxation times from FPDM approach -  $T_{1z}$  and  $T_{1x}$ , compared with those estimated by the EY relation (Eq. 7) -  $T_{1z}^{\text{EY}}$  and  $T_{1x}^{\text{EY}}$  with different  $t^{\text{deg}}$ . Note that  $T_{1x}^{\text{EY}}$  values with  $t^{\text{deg}}=10^{-6}$  eV are multiplied by 100. (d) The anisotropy ratios of  $T_1$  and  $T_1^{\text{EY}}$  with different  $t^{\text{deg}}$ .

than FPDM values of  $T_{1x}$  by 3-4 orders of magnitude and the temperature dependence of  $T_{1z}^{\text{EY}}$  is not consistent with FPDM  $T_{1z}$ . Moreover, from Fig. 3(d), we find that  $T_{1z}^{\text{EY}}/T_{1x}^{\text{EY}}$  are in agreement with and completely different from FPDM  $T_{1z}/T_{1x}$  when  $t^{\text{deg}}$  is  $10^{-3}$  and  $10^{-6}$  eV respectively. We have also checked the EY relation with other  $t^{\text{deg}}$ . As expected, we find that  $t^{\text{deg}}=10^{-2}$  eV leads to quite similar results to  $t^{\text{deg}}=10^{-3}$  eV, but  $t^{\text{deg}}=10^{-8}$  eV leads to unreasonable  $T_1^{\text{EY}}$ .

Therefore, from Fig. 3(c) and (d), we conclude that the EY relation works qualitatively with relatively large  $t^{\text{deg}}$  but fails with tiny  $t^{\text{deg}}$  for the zero-filed spin relaxation in graphite due to the spin-orbit-phonon interaction. This conclusion can be explained within the density-matrix master equation approach: The use of the EY relation re-

quires that spin relaxation is well described by FGR with spin-flip transitions. According to Appendix C, to obtain a FGR-type formula (Eq. 23) from the density-matrix master equation, it is required that  $s_\alpha$  can be safely replaced by  $s_\alpha^{\text{deg}}$  for bands near  $E_F$ , which ensures that spin-up and spin-down are well defined for all electronic states (in the new basis diagonalizing  $s_\alpha^{\text{deg}}$ ). However, in general, the off-diagonal element of  $s_\alpha$  between two states with a finite energy difference is not negligible, especially when the energy difference is small. Therefore, replacing  $s_\alpha$  by  $s_\alpha^{\text{deg}}$  with a tiny  $t^{\text{deg}}$  may lead to significant errors. A simple solution of this problem is increasing  $t^{\text{deg}}$  and it seems reasonable to set  $t^{\text{deg}}$  comparable to or a bit smaller than  $k_B T$  (see Appendix C.3).

## ACKNOWLEDGMENTS

This work is supported by National Natural Science Foundation of China (Grant No. 12304214), Fundamental Research Funds for Central Universities (Grant No. JZ2023HGPA0291). This research used resources of the HPC Platform of Hefei University of Technology.

## APPENDICES

### Appendix A: The generalized scattering-rate matrix $P$

We use the following form of  $P$ , which is called the Lindbladian form here and reads[10, 11]

$$P_{1234} = \frac{2\pi}{\hbar} \sum_{q\lambda\pm} G_{13}^{q\lambda\pm} G_{24}^{q\lambda\pm,*} n_{q\lambda}^{\pm}, \quad (8)$$

$$G_{13}^{q\lambda\pm} = g_{12}^{q\lambda\pm} \sqrt{\delta_{\sigma}^G (\epsilon_1 - \epsilon_2 \pm \omega_{q\lambda})}, \quad (9)$$

where  $q$  and  $\lambda$  are phonon wavevector and mode,  $g^{q\lambda\pm}$  is the e-ph matrix element, resulting from the absorption (−) or emission (+) of a phonon, computed with self-consistent SOC from first principles,[20]  $n_{q\lambda}^{\pm} = n_{q\lambda} + 0.5 \pm 0.5$  in terms of phonon Bose factors  $n_{q\lambda}$ , and  $\delta_{\sigma}^G$  represents an energy conserving  $\delta$ -function broadened to a Gaussian of width  $\sigma$ .

According to Ref. 14, there exists another pathway to arrive at the Markov limit of the scattering term, leading to another form of  $P$ , called the conventional form here. The conventional form contains a single Dirac delta function and reads

$$P_{1234} = \sum_{q\lambda\pm} a_{13}^{q\lambda\pm} b_{24}^{q\lambda\pm,*}, \quad (10)$$

$$a_{13}^{q\lambda\pm} = \frac{1}{\hbar} g_{13}^{q\lambda\pm} \sqrt{n_{q\lambda}^{\pm}}, \quad (11)$$

$$b_{13}^{q\lambda\pm} = 2\pi g_{13}^{q\lambda\pm} \sqrt{n_{q\lambda}^{\pm}} \delta(\omega_{13} \pm \omega_{q\lambda}). \quad (12)$$

The conventional form of  $P$  was widely employed in previous theoretical simulations of spin dynamics based on the density-matrix master equation approach.[2] It however does not preserve the positive-definite character of the occupation numbers or the diagonal elements of  $\rho$ , unlike the Lindbladian form,[14] although we find that two forms of  $P$  lead to rather similar  $\tau_s$  (within 10% for graphite and within 20% for various other materials) and the same carrier lifetime  $\tau_p$ . Therefore, we will stick to the Lindbladian form of  $P$ .

The smearing parameter  $\sigma$  in the Lindbladian form has a weak physical meaning and roughly corresponds to the collision duration or  $\tau_p$ .  $\sigma$  is set comparable to  $k_B T$ , which is a few times larger than  $\tau_p$ , to speed up the k-point convergence. Our numerical tests show that the

resulting  $T_1$  values are not sensitive to  $\sigma$ . For example, the resulting  $T_1$  is only changed by a few percent when  $\sigma$  is reduced to its half.

### Appendix B: Spin lifetime

$\rho(t)$  can be separated as

$$\rho_{kmn}(0) = f_{km} \delta_{mn} + \delta\rho_{kmn}(0), \quad (13)$$

where  $f_{km}$  is the Fermi-Dirac occupation of state  $(k, m)$ .  $\delta\rho(t)$  is the excess density matrix and typically small in a spin-relaxation simulation.

Suppose the initial time is  $t = 0$ , starting from an initial excess density matrix  $\delta\rho(0)$  prepared with a net excess spin along the direction  $\alpha$ , we evolve  $\rho(t)$  through Eq. 1 for a long enough time, typically a few ns. We then obtain the excess spin observable along the direction  $\alpha$  -  $S_{\alpha}^{\text{ex}}(t)$  from  $\delta\rho(t)$  through

$$S_{\alpha}^{\text{ex}}(t) = \text{Tr}[\delta\rho(t) s_{\alpha}]. \quad (14)$$

Then  $T_{1\alpha}$  is extracted by fitting  $S_{\alpha}^{\text{ex}}(t)$  using the exponential decay curve:

$$S_{\alpha}^{\text{ex}}(t) = S_{\alpha}^{\text{ex}}(0) \exp\left(-\frac{t}{T_1}\right). \quad (15)$$

As we have checked, the results of  $T_{1\alpha}$  are almost unchanged if the length of time evolution is increased from a few ns to a few hundreds of ns. This is because the time evolution of  $S_{\alpha}^{\text{ex}}(t)$  fits Eq. 15 excellently even at the first few ps for graphite.

### Appendix C: The approximate formula of $T_1$ and FGR

An alternative form of the initial excess density matrix  $\delta\rho(0)$  is

$$\delta\rho_{kmn}(0) = \delta\rho_{kmn}^{s_{\alpha}}, \quad (16)$$

$$\delta\rho_{kmn}^{s_{\alpha}} = \frac{\mu_B g_0 \delta B}{\hbar} s_{\alpha, kmn} \left( \frac{\Delta f}{\Delta \epsilon} \right)_{kmn}, \quad (17)$$

$$\left( \frac{\Delta f}{\Delta \epsilon} \right)_{kmn} = f'_{km} \delta_{\epsilon_{km} \epsilon_{kn}} + \frac{f_{km} - f_{kn}}{\epsilon_{km} - \epsilon_{kn}} (1 - \delta_{\epsilon_{km} \epsilon_{kn}}), \quad (18)$$

where  $\delta\rho^{s_{\alpha}}$  is the density-matrix change induced by a spin Zeeman Hamiltonian  $H^{sZ} = \mu_B g_0 \delta B s_{\alpha}$  with a perturbation magnetic field  $\delta B$  along the direction  $\alpha$ . [7]  $s_{\alpha}$  is spin Pauli matrix in Blöch basis along direction  $\alpha$ .

*Appendix C.1: The approximate formula of  $T_1$  with  $\delta\rho^{s_{\alpha}}$*

Due to the inversion symmetry of graphite (and each layer of it), there are no SOC-induced band splittings

and no  $k$ -dependent effective SOC fields (called “internal magnetic fields”). Therefore, Larmor spin precession, caused by the coherent term of the master equation Eq. 1, should be insignificant. Considering that spin relaxation is mainly determined by the scattering strength and Larmor precession frequency,[1, 2] the coherent term is probably unimportant to spin relaxation in graphite and can be approximately neglected.

Without Larmor precession, we may assume that the excess density matrix  $\delta\rho(t)$  is approximately proportional to  $\delta\rho^{s_\alpha}$  given above (Eq. 17) at any  $t$ , if initially we take  $\delta\rho(0) = \delta\rho^{s_\alpha}$ . This is a nature choice of  $\delta\rho(t)$  for the simulation of  $T_{1\alpha}$  due to several reasons: (i) The instantaneous spin relaxation rates  $T_1^{-1}$  at any  $t$  are the same if  $\delta\rho = \lambda\delta\rho^{s_\alpha}$  with  $\lambda$  a constant and  $\lambda \leq 1$ . (ii)  $\delta\rho^{s_\alpha}$  leads to high spin polarizations along the direction  $\alpha$  but no excess charges at every  $k$ -point. (iii) The matrix elements  $\delta\rho_{kmn}$  are large and negligible when states  $(k, m)$  and  $(k, n)$  are both near and far from  $E_F$  respectively, consistent with the facts that  $T_1$  is a Fermi-surface property and the e-ph scattering processes are only significant with partial occupations. Therefore,  $T_{1\alpha}$  can be approximately computed from

$$\frac{dS_\alpha^{\text{ex}}}{dt} = -\frac{S_\alpha^{\text{ex}}}{T_{1\alpha}}, \quad (19)$$

$$S_\alpha^{\text{ex}} = \text{Tr}[\delta\rho^{s_\alpha} s_\alpha]. \quad (20)$$

Using the above equations and Eq. 1 without the coherent term, we obtain the approximate formula of  $T_{1\alpha}^{-1}$ ,

$$T_{1\alpha}^{-1} = \frac{2\pi}{\hbar N_k^2 S_\alpha^{\text{ex}}} \text{Tr}_n \text{Re} \sum_{kk'\lambda} [s_\alpha, G^{q\lambda-}]_{kk'} \times \left[ \begin{array}{l} (\delta\rho^{s_\alpha})_k G_{kk'}^{q\lambda-} (n_{q\lambda} + I - f_{k'}) \\ -(n_{q\lambda} + f_k) G_{kk'}^{q\lambda-} (\delta\rho^{s_\alpha})_{k'} \end{array} \right]^\dagger_n. \quad (21)$$

Here, the  $G$  is exactly as defined above in Eq. 9, but separating the wave vector indices  $(k, k')$  and writing it as a matrix in the space of band indices  $(n, n')$  alone. Similarly,  $s_\alpha$  and  $\delta\rho^{s_\alpha}$  are also matrices in the band space,  $\text{Tr}_n$  and  $\dagger_n$  are trace and Hermitian conjugate in band space, and  $[o, G]_{kk'} \equiv o_k G_{kk'} - G_{kk'} o_{k'}$ , written using matrices in band space. Eq. 21 is the same as Eq. 3 in Ref. 7.

### Appendix C.2: FGR

If the bands near  $E_F$  are all degenerate or the matrix elements  $s_{\alpha,kmn}$  with  $\epsilon_{km} \neq \epsilon_{kn}$  are all negligible., the spin matrix  $s_\alpha$  in  $\delta\rho^{s_\alpha}$  (Eq. 17) can be safely replaced by its degenerate-subspace projection  $s_\alpha^{\text{deg}}$ , whose matrix elements satisfy  $s_{\alpha,kmn}^{\text{deg}} = s_{\alpha,kmn} \delta_{\epsilon_{km}\epsilon_{kn}}$ . In such cases, we can further simplify Eq. 21 to the FGR-like expression

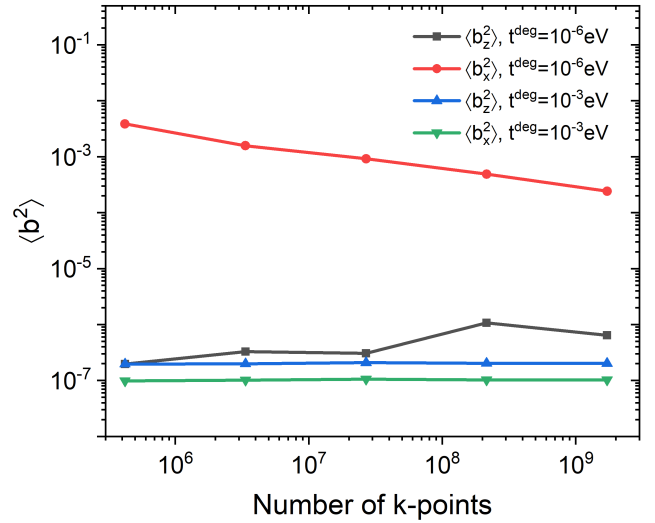


FIG. 4.  $\langle b^2 \rangle$  as a function of number of  $k$ -points. The uniform  $k$  meshes  $18N \times 18N \times 6N$  with  $N$  an integer are used for  $\langle b^2 \rangle$  simulations.

(the derivation is given in SI of Ref. 7),

$$T_{1\alpha}^{-1} = \frac{2\pi}{\hbar N_k^2 S_\alpha^{\text{ex}} k_B T} \sum_{kk'\lambda \pm nn'} \left\{ \left| [s_\alpha^{\text{deg}}, g^{q\lambda-}]_{knk'n'} \right|^2 \delta(\epsilon_{kn} - \epsilon_{k'n'} - \omega_{q\lambda}) f_{k'n'} (1 - f_{kn}) n_{q\lambda} \right\}. \quad (22)$$

In the new basis obtained by diagonalizing  $s_\alpha$  or  $s_\alpha^{\text{deg}}$  within degenerate subspaces, the above equation becomes

$$T_{1\alpha}^{-1} = \frac{2\pi}{\hbar N_k^2 S_\alpha^{\text{ex}} k_B T} \times \sum_{kk'\lambda \pm nn'} \left\{ \left| (S_{\alpha,kn}^{\text{exp}} - S_{\alpha,k'n'}^{\text{exp}}) g_{knk'n'}^{q\lambda-} \right|^2 \delta(\epsilon_{kn} - \epsilon_{k'n'} - \omega_{q\lambda}) f_{k'n'} (1 - f_{kn}) n_{q\lambda} \right\}, \quad (23)$$

where  $S_{\alpha,kn}^{\text{exp}}$  is the spin expectation value along the direction  $\alpha$  and  $S_{\alpha,kn}^{\text{exp}} \equiv s_{\alpha,knkn}$  (in the new basis).

In many systems such as conduction bands of silicon and monolayer  $\text{MoS}_2$ , the values of  $S_{\alpha,kn}^{\text{exp}}$  are either  $\approx 0.5\hbar$  or  $\approx -0.5\hbar$ . In such systems, according to Eq. 23, only the spin-flip transitions between two states with opposite signs of  $S_{\alpha,kn}^{\text{exp}}$  have non-negligible contributions to  $T_{1\alpha}^{-1}$ . Then, Eq. 23 becomes a FGR-type formula with initial and final states having opposite signs of  $S_{\alpha,kn}^{\text{exp}}$ , corresponding to spin-flip transitions.

### Appendix C.3: The degeneracy threshold

When the coherent dynamics is unimportant to spin relaxation, *ab initio* results of  $T_1$  calculated by Eq. 21 with  $\delta\rho^{s_\alpha}$  have been found close to the FPDM results (Eq. 1) for various materials including graphite. However, the

FGR-like formulas (Eqs. 22 and 23) may lead to significant errors, if the degeneracy threshold  $t^{\text{deg}}$  is too small. This is because replacing  $s_\alpha$  in  $\delta\rho^{s_\alpha}$  (Eq. 17) by  $s_\alpha^{\text{deg}}$  with too small  $t^{\text{deg}}$  is problematic in some cases, where the matrix elements  $s_{\alpha,kmn}$  with  $\epsilon_{km} \neq \epsilon_{kn}$  are not negligible. In such cases, when  $\epsilon_{km}$  and  $\epsilon_{kn}$  are both near  $E_F$  and  $|\epsilon_{km} - \epsilon_{kn}|$  is a few  $k_B T$  or smaller, the matrix element  $\left(\frac{\Delta f}{\Delta \epsilon}\right)_{kmn}$  in  $\delta\rho^{s_\alpha}$  is not much smaller than  $\frac{df}{d\epsilon}|_{\epsilon=\bar{\epsilon}}$  with  $\bar{\epsilon} = \frac{\epsilon_{km} + \epsilon_{kn}}{2}$ , so that neglecting the off-diagonal matrix element  $\delta\rho_{kmn}^{s_\alpha}$  is problematic and replacing  $s_\alpha$  in  $\delta\rho^{s_\alpha}$  by  $s_\alpha^{\text{deg}}$  with too small  $t^{\text{deg}}$  is improper.

Considering that  $\left(\frac{\Delta f}{\Delta \epsilon}\right)_{kmn}$  varies relatively slow with the variation of  $|\epsilon_{km} - \epsilon_{kn}|$  (in the scale of a few  $k_B T$ ), a simple way to fix the above degeneracy issue is using a relatively large  $t^{\text{deg}}$ , comparable to or a bit smaller than  $k_B T$ , for Eqs. 22 and 23.

#### Appendix D: Computational details

The ground-state electronic structure, phonons, as well as the e-ph matrix elements are firstly calculated using density functional theory (DFT) with relatively coarse  $k$  and  $q$  meshes in the DFT plane-wave code JDFTx[21]. We use the experimental lattice constants with  $a=2.76$  Å and  $c=6.71$  Å, which are close to the relaxed lattice constants. The exchange-correlation functional is PBE[22]. The internal ge-

ometries are fully relaxed using the DFT+D3 method for van der Waals dispersion corrections[23]. We use Optimized Norm-Conserving Vanderbilt (ONCV) pseudopotentials[24] with self-consistent SOC throughout, which we find converged at a kinetic energy cutoff of 74 Ry. The DFT calculations use  $18 \times 18 \times 6$   $k$  meshes. The phonon calculation employs a  $6 \times 6 \times 2$  supercell through finite difference calculations.

We then transform all quantities from plane wave basis to maximally localized Wannier function basis[25], and interpolate[20] them to substantially finer  $k$  and  $q$  meshes. The fine  $k$  and  $q$  meshes are typically  $252 \times 252 \times 84$ . We have checked the  $k$ -point convergence carefully.  $252 \times 252 \times 84$   $k$  meshes are found fine enough to converge  $\langle b^2 \rangle$  results with  $t^{\text{deg}} \geq 10^{-4}$  eV and  $T_1$  results within 5% and 20% respectively. Finer  $k$  meshes do not change the trends of these results. However, we find that  $\langle b^2 \rangle$  results with  $t^{\text{deg}} \leq 10^{-6}$  eV are very sensitive to  $k$  meshes and even  $1728 \times 1728 \times 576$   $k$  meshes are not enough to converge them. We show  $\langle b^2 \rangle$  as a function of number of  $k$ -points in Fig. 4. It seems impractical to fully converge  $\langle b^2 \rangle$  results with  $t^{\text{deg}} \leq 10^{-6}$  eV. Our  $k$ -point convergence tests indicate that tiny values of  $t^{\text{deg}}$  are not suitable for numerical calculations of  $\langle b^2 \rangle$ . The real-time dynamics simulations are done with our own developed DMD code interfaced to JDFTx.

#### REFERENCE

- 
- [1] I. Žutić, J. Fabian, and S. D. Sarma, Spintronics: Fundamentals and Applications, *Rev. Mod. Phys.* **76**, 323 (2004).
  - [2] M. Wu, J. Jiang, and M. Weng, Spin dynamics in semiconductors, *Phys. Rep.* **493**, 61 (2010).
  - [3] A. Avsar, H. Ochoa, F. Guinea, B. Özyilmaz, B. J. van Wees, and I. J. Vera-Marun, Colloquium: Spintronics in Graphene and Other Two-Dimensional Materials, *Rev. Mod. Phys.* **92**, 021003 (2020).
  - [4] L. E. Hueso, J. M. Pruneda, V. Ferrari, G. Burnell, J. P. Valdés-Herrera, B. D. Simons, P. B. Littlewood, E. Artacho, A. Fert, and N. D. Mathur, Transformation of spin information into large electrical signals using carbon nanotubes, *Nature* **445**, 410 (2007).
  - [5] T. Banerjee, W. G. van der Wiel, and R. Jansen, Spin injection and perpendicular spin transport in graphite nanostructures, *Phys. Rev. B* **81**, 214409 (2010).
  - [6] A. Habib, J. Xu, Y. Ping, and R. Sundararaman, Electric fields and substrates dramatically accelerate spin relaxation in graphene, *Phys. Rev. B* **105**, 115122 (2022).
  - [7] J. Xu, A. Habib, S. Kumar, F. Wu, R. Sundararaman, and Y. Ping, Spin-Phonon Relaxation from a Universal Ab Initio Density-Matrix Approach, *Nat. Commun.* **11**, 2780 (2020).
  - [8] B. Márkus, M. Gmitra, B. Dóra, G. Csósz, T. Fehér, P. Szirmai, B. Náfrádi, V. Zólyomi, L. Forró, J. Fabian, *et al.*, Ultralong 100 ns spin relaxation time in graphite at room temperature, *Nat. Commun.* **14**, 2831 (2023).
  - [9] J. Fabian and S. D. Sarma, Spin relaxation of conduction electrons in polyvalent metals: Theory and a realistic calculation, *Phys. Rev. Lett.* **81**, 5624 (1998).
  - [10] J. Xu and Y. Ping, Ab initio predictions of spin relaxation, dephasing, and diffusion in solids, *J. Chem. Theory Comput.* **20**, 492 (2023).
  - [11] J. Xu, A. Habib, R. Sundararaman, and Y. Ping, Ab initio ultrafast spin dynamics in solids, *Phys. Rev. B* **104**, 184418 (2021).
  - [12] J. Xu and H. Xiao, Ab initio wannier-representation-based calculations of photocurrent in semiconductors and metals, *Phys. Rev. B* (2024).
  - [13] J. Xu, K. Li, U. N. Huynh, M. Fadel, J. Huang, R. Sundararaman, V. Vardeny, and Y. Ping, How spin relaxes and dephases in bulk halide perovskites, *Nat. Commun.* **15**, 188 (2024).
  - [14] R. Rosati, R. C. Iotti, F. Dolcini, and F. Rossi, Derivation of Nonlinear Single-Particle Equations via Many-Body Lindblad Superoperators: A Density-Matrix Approach, *Phys. Rev. B* **90**, 125140 (2014).
  - [15] J. Xu, H. Takenaka, A. Habib, R. Sundararaman, and Y. Ping, Giant spin lifetime anisotropy and spin-valley locking in silicene and germanene from first-principles density-matrix dynamics, *Nano Lett.* **21**, 9594 (2021).
  - [16] J. Xu and Y. Ping, Substrate effects on spin relaxation in two-dimensional dirac materials with strong spin-orbit



- coupling, *npj Comput. Mater.* **9**, 47 (2023).
- [17] W. Leyland, R. Harley, M. Henini, A. Shields, I. Farrer, and D. Ritchie, Oscillatory dyakonov-perel spin dynamics in two-dimensional electron gases, *Phys. Rev. B* **76**, 195305 (2007).
- [18] O. D. Restrepo and W. Windl, Full first-principles theory of spin relaxation in group-iv materials, *Phys. Rev. Lett.* **109**, 166604 (2012).
- [19] M. Droger, C. Franzen, F. Volmer, T. Pohlmann, L. Banszerus, M. Wolter, K. Watanabe, T. Taniguchi, C. Stampfer, and B. Beschoten, Spin lifetimes exceeding 12 ns in graphene nonlocal spin valve devices, *Nano Lett.* **16**, 3533 (2016).
- [20] F. Giustino, Electron-Phonon Interactions from First Principles, *Rev. Mod. Phys.* **89**, 015003 (2017).
- [21] R. Sundararaman, K. Letchworth-Weaver, K. A. Schwarz, D. Gunceler, Y. Ozhages, and T. A. Arias, JDFTx: Software for Joint Density-Functional Theory, *SoftwareX* **6**, 278 (2017).
- [22] J. P. Perdew, K. Burke, and M. Ernzerhof, Generalized Gradient Approximation Made Simple, *Phys. Rev. Lett.* **77**, 3865 (1996).
- [23] S. Grimme, J. Antony, S. Ehrlich, and H. Krieg, A consistent and accurate ab initio parametrization of density functional dispersion correction (dft-d) for the 94 elements h-pu, *J. Chem. Phys.* **132** (2010).
- [24] D. R. Hamann, Optimized Norm-Conserving Vanderbilt Pseudopotentials, *Phys. Rev. B* **88**, 085117 (2013).
- [25] N. Marzari and D. Vanderbilt, Maximally Localized Generalized Wannier Functions for Composite Energy Bands, *Phys. Rev. B* **56**, 12847 (1997).